Optics and Lasers in Engineering 151 (2022) 106920

Contents lists available at ScienceDirect

Optics and Lasers in Engineering

journal homepage: www.elsevier.com/locate/optlaseng

Sensitive detection of orthogonal polarization intensity ratio via metal-cladding waveguide

Hongrui Shan [a], Qiheng Wei [a], Hailang Dai [a,*], Xianfeng Chen [a,b,c,d,*]

[a] State Key Laboratory of Advanced Optical Communication Systems and Networks, School of Physics and Astronomy, Shanghai Jiao Tong University, Shanghai 200240, China
[b] Shanghai Research Center for Quantum Sciences, Shanghai 201315, China
[c] Jinan Institute of Quantum Technology, Jinan 250101, China
[d] Collaborative Innovation Center of Light Manipulation and Applications, Shandong Normal University, Jinan 250358, China

ARTICLE INFO

Keywords:
Metal-cladding waveguide
Ultrahigh order modes
Detection of polarization
Polarized beam analyzer

ABSTRACT

A rapid and sensitive detection method of incident light with different orthogonal polarization intensity ratios based on the double metal-cladding waveguide has been demonstrated. The middle layer of the waveguide is a uniaxial negative crystal lithium niobate, resulting in distinct coupling angles for TE and TM polarization. The isolation of the device can reach 42 dB due to well separation of TE and TM polarization. The quantitative experiments to measure ratio of TE to TM incident light have been carried out. Meanwhile, this method can support polarization detection in ultraviolet, visible, and infrared region. This method will play a significant role in optical information processing system and the integrated system.

1. Introduction

Polarized beam intensity ratio analyzer (PBA), which is a basic optical element to detect the polarization of the incident light, plays a critical role in the photonics system [1]. Over the past decades, several PBAs has been reported in papers [2–18]. There are bulk-type structures [2–6], grating-type structures [7–10], fiber-type structures [11–13], and waveguide-type structures [14–17]. As is well known, the conventional bulk-type PBA is popular in free-space optical signal processing. However, the cumbersome is a significant disadvantage of traditional bulk-type PBA, indicating that it is infeasible for application and integration. Therefore, the PBA based-on grating-type has been produced in recent years, which can offer desirable performance of polarization modulation owning to its light weight and small size. Nevertheless, the grating-type PBA is hard to be applied to the field of communications due to high loss and harsh process requirements. In general, the fiber-type PBA is widely utilized in communications. It has excellent transmission characteristics that makes it convenient for communications. However, it is difficult to be designed and fabricated with highly sensitive of detection. Thus, producing an especially high-performance PBA suiting for large-scale application in the integrated system is a fiercely desire.

Actually, the waveguide technology provides a chance due to the distinct advantages, such as small size, low weight, stable, reliable performance, and easy integration [14–18]. It is of great interests to implement the PBA by utilizing the waveguide. The double metal-cladding waveguide (DMCW), can excite the ultrahigh-order guided modes (UOMs) which have many outstanding properties, for example, high modes density in guided layer, small propagation constant of light, free-space coupling into guided layer at small incident angle, highly sensitive detection of weakly refractive index and so on [19–22]. Based on these unique properties, the DMCW has been used to many achievements in sensors and actuators [23–34].

In this letter, we demonstrate a new type PBA based on the DMCW, which achieves sensitive detection of different orthogonal polarization intensity ratios due to distinguishing the TE/TM polarization via the coupling efficiency of light in waveguide. The DMCW has three-layer structure and the middle-guided layer is a uniaxial negative crystal lithium niobate (LN) which has different refractive indices for orthogonal eigen-polarizations, the ordinary o and extraordinary e states.

In this DMCW, TE and TM polarization resonate at many different coupling angles. Hence, when the incident light meets the resonance angle of one polarization mode, it will be fully coupled into the guided layer of DMCW, and the other polarization mode will be completely reflected. Meanwhile, the TE/TM polarization light will excite different modes in DMCW at corresponding incident angle which is coupling angle, respectively. In addition, the difference coupling angle between TE and TM is only 0.01° that can be distinguished by DMCW. Moreover, our PBA is able to support large wavelength range and wide-angle extent.

* Corresponding authors.
E-mail addresses: hailangdai@sjtu.edu.cn (H. Dai), xfchen@sjtu.edu.cn (X. Chen).

https://doi.org/10.1016/j.optlaseng.2021.106920
Received 3 August 2021; Received in revised form 28 October 2021; Accepted 10 December 2021

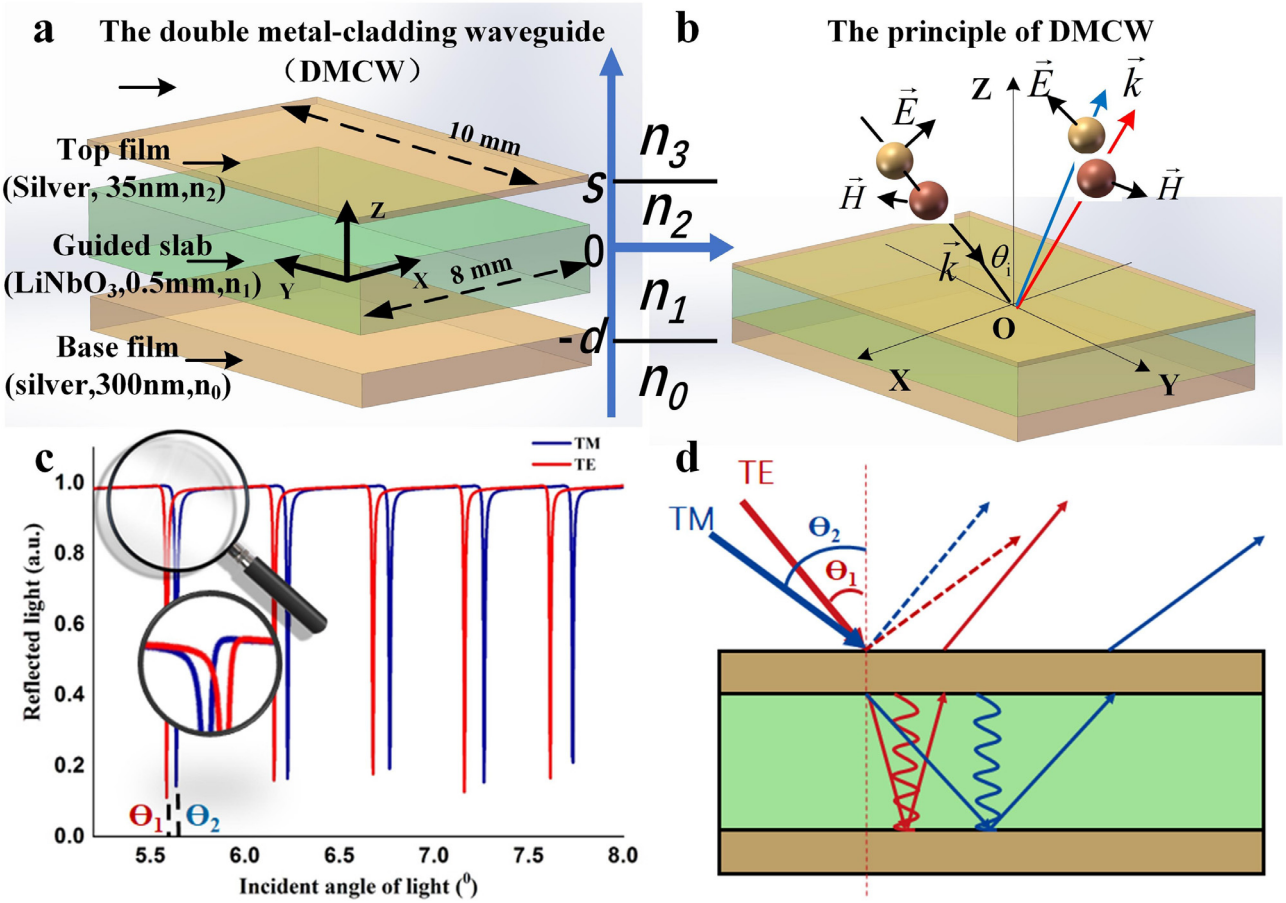

Fig. 1. (a) Schematic of double metal-cladding waveguide (DMCW). (b)The mode exciting principle of DMCW. (c) Simulated reflected light spectrum of TE and TM modes with respect to the incident angles. The calculation is performed by ATR software designed by our team. (d) The diagrammatic drawing of DMCW with incident lights at θ_1 and θ_2 corresponding to (c). (d) Schematics of the PBA system based on DMCW.

2. Method

The DMCW has many more fascinating characteristics than the traditional all-dielectric waveguide. One of the most significant characteristics is the existing of UOMs at small incident angles θ_i. Hence, the effective refractive index of UOMs $N_{eff} = n\sin\theta_i \to 0$ (θ_i<1°) enable the cavity to decrease modes space, resulting that a sub-mm DMCW can excite more than 1000 modes.

The DMCW is a three-layer waveguide. A dielectric slab with thickness d and dielectric constant ε_1 acting as the guided layer is sandwiched by thermal evaporation sputtering two metal films, which serve as the coupling layer and the substrate, respectively. As shown in Fig. 1(a), considering a situation in which $\mathrm{Re}(n_2) = \mathrm{Re}(n_0) < n_3 < n_1$, we assume two Ag films (layer 0 and layer 2) extend at infinity and the width of guiding layer 1 is much greater than its thickness. Then we can consider the electric field in waveguide is confined in only one direction such as x direction. And the geometric structure and refractive index distribution of the waveguide are assumed to be constant in y direction. For guided modes, the electric fields in substrate layer 0 and coating layer 2 attenuate exponentially, but in guided layer 1 and air layer 3 oscillate periodicity. It consists two waves propagating in opposite directions (TE and TM polarizations). Consequently, for TE polarization, the electric field in the waveguide can be expressed as

$$E_y(z) = \begin{cases} A_3\exp\left(-i\kappa_3(z-s)\right) + B_3\exp\left(i\kappa_3(z-s)\right), s < z < +\infty \\ A_2\exp\left(-p_2 z\right) + B_2\exp\left(p_2 z\right), 0 < z < s \\ A_1\exp\left(-i\kappa_1 z\right) + B_1\exp\left(i\kappa_1 z\right), -d < z < 0 \\ A_0\exp\left(p_0(z+d)\right), -\infty < z < -d \end{cases} \quad (1)$$

where

$$\begin{cases} \kappa_1 = (k_0{}^2 n_1{}^2 - \beta^2)^{1/2} \\ \kappa_3 = (k_0{}^2 n_3{}^2 - \beta^2)^{1/2} \\ p_0 = (\beta^2 - k_0{}^2 n_0{}^2)^{1/2} \\ p_2 = (\beta^2 - k_0{}^2 n_2{}^2)^{1/2} \end{cases} \quad (2)$$

$k_0 = 2\pi/\lambda$ is the propagation constant in vacuum and $\beta = k_0 n_1 \sin\theta$ is the x component of the wave vector k. x direction is along the propagation direction in waveguide. Using the continuity condition of $E_y$and $\partial E_y/\partial z$ at boundaries $z = 0$, $z = s$, and $z = -d$ (as shown in Fig. 1(a)), the reflection coefficient r can be expressed as

$$r^{TE} = \frac{B_3}{A_3} = \frac{r_{32}{}^{TE} + r_{210}{}^{TE}\exp(-2p_2 s)}{1 + r_{32}{}^{TE} r_{210}{}^{TE}\exp(-2p_2 s)} \quad (3)$$

where

$$\begin{cases} r_{32}{}^{TE} = \exp(-2i\phi_{32}) \\ r_{210}{}^{TE} = \dfrac{\exp(-2i\phi_{12}{}^{TE}) - \exp(2i(\kappa_1 d - \phi_{10}{}^{TE}))}{\exp(2i(\kappa_1 d - \phi_{10}{}^{TE} - \phi_{12}{}^{TE})) - 1} \\ \phi_{10}{}^{TE} = \tan^{-1}\left(\dfrac{p_0}{\kappa_1}\right) \\ \phi_{12}{}^{TE} = \tan^{-1}\left(\dfrac{p_2}{\kappa_1}\right) \\ \phi_{32}{}^{TE} = \tan^{-1}\left(\dfrac{p_2}{\kappa_3}\right) \end{cases} \quad (4)$$

r_{32} and r_{210} are coefficients without meaning which are created to acquire a clear result. The reflectivity R^{TE} is equal to$r^{TE} r^{TE} *= |r^{TE}|^2$.

And for TM polarization, the magnetic field in the waveguide can be expressed as

$$H_y(z) = \begin{cases} C_3 \exp\left(-i\kappa_3(z-s)\right) + D_3 \exp\left(i\kappa_3(z-s)\right), s < z < +\infty \\ C_2 \exp\left(-p_2 z\right) + D_2 \exp\left(p_2 z\right), 0 < z < s \\ C_1 \exp\left(-i\kappa_1 z\right) + D_1 \exp\left(i\kappa_1 z\right), -d < z < 0 \\ C_0 \exp\left(p_0(z+d)\right), -\infty < z < -d \end{cases} \tag{5}$$

With the continuity condition of $E_z$and H_y at boundaries$z = 0$, $z = s$, and $z = -d$, the reflection coefficient r can be expressed as

$$r^{TM} = \frac{D_3}{C_3} = \frac{{r_{32}}^{TM} + {r_{210}}^{TM} \exp(-2p_2 s)}{1 + {r_{32}}^{TM}{r_{210}}^{TM} \exp(-2p_2 s)} \tag{6}$$

where

$$\begin{cases} {r_{32}}^{TM} = \exp(-2i{\phi_{32}}^{TM}) \\ {r_{210}}^{TM} = \dfrac{\exp(-2i{\phi_{12}}^{TM}) - \exp(2i(\kappa_1 d - {\phi_{10}}^{TM}))}{\exp(2i(\kappa_1 d - {\phi_{10}}^{TM} - {\phi_{12}}^{TM})) - 1} \\ {\phi_{10}}^{TM} = \tan^{-1}\left(\dfrac{{n_1}^2 p_0}{{n_0}^2 \kappa_1}\right) \\ {\phi_{12}}^{TM} = \tan^{-1}\left(\dfrac{{n_1}^2 p_2}{{n_2}^2 \kappa_1}\right) \\ {\phi_{32}}^{TM} = \tan^{-1}\left(\dfrac{{n_3}^2 p_2}{{n_2}^2 \kappa_3}\right) \end{cases} \tag{7}$$

Therefore, the reflectivity of TM polarization is obviously different to the TE polarization with the same incident angle. The total reflectivity of an incident beam is in a one-to-one correspondence with the intensity ratio of TE and TM. As a result, the measuring the polarization intensity ratio is achieved by monitoring the reflected light intensity.

In our experiments, the configuration of DMCW is illustrated in Fig. 1(a). A 500 μm thickness of LN crystal serves as guided layer, and a 35 nm thin silver upper film layer is used to couple the incident light into the guided layer. The third layer is a 300 nm thick silver film used as substrate layer, which prevents the leakage of light. As depicted in Fig. 1(b), the upper thin silver film is used to couple incident light and excite and the UOMs. The DMCW is easy to be excited by free-space coupling due to the small effective refractive index N_{eff}.

For an anisotropic guided layer, DMCW becomes polarization-dependent due to birefringence of the guided medium. In experiment, the optical axis of LN is along Z direction, which causes the DMCW to be sensitive to the polarization of incident light. When the light illuminates on the upper layer of the DMCW, the UOMs will be excited at the coupling angle. As shown in Fig. 1(c), according to the dispersion Eq. (3) and (6), we simulate the reflected light spectrum of DMCW for both TE and TM polarization incident lights at the wavelength of 632.8 nm. The reflected light spectrum varies with the incident angle, and it demonstrates that the DMCW can support different TE and TM modes with particular angles. When the beam illuminates at a coupling angle θ_1, almost all power of incident light is coupled into the DMCW. Then attenuated total reflection (ATR) of which full width at half maximum (FWHM) is 0.01° will appear on the reflected light spectrum (indicated in red line). If the angle of incident light is changed to another coupling angle θ_2, it leads to another set of modes in DMCW (indicated in blue line) as shown in Fig. 1(d). Thus, we can scan the angle of incident light between two angles at least existing one TE coupling angle (for example θ_1) and the adjacent TM coupling angle (for example θ_2). The distinct guided modes in DMCW will provide the polarization information of the incident light. Furthermore, TE and TM incident light can be distinguished by the DMCW as long as the difference between their coupling angles (θ_2 to θ_1) is more than 0.01°, and in experiments the difference is usually 0.1°, which is well beyond resolution limit of DMCW.

3. Experiment results

Fig. 2 shows the schematic structure of the proposed configuration, in this experiment. The He-Ne laser (632.8 nm, 25 mW, USA) is used to excite the UOMs in the DMCW. Two apertures with diameters of 1 mm are inserted to collimate the incident light. The polarizer and quarter wave plate are employed to transform the circular polarized incident light into various polarized beams, which will be detected by the PBA based on DMCW. The DMCW is vertically located on a computer-controlled goniometer that can adjust the incident angle precisely. As the beam illuminates on the DMCW, the UOMs are excited, and the reflected light will be collected by the detector on the $\theta/2\theta$ goniometer. In experiment, a polarized beam splitter with optical power meters and a polarimeter (THORLABS PAX1000) are used to guarantee accurate measurement of TE and TM components which can serve as a standard value.

There are 5 different polarized beams used to illuminate on the DMCW, respectively, including linear TM polarization, linear TE polarization, circular polarization (TE/TM=1), and two elliptic Polarizations (TM/TE>1 and TM/TE<1). The five corresponding reflected light spectrums are shown in Fig. 3. The incident light ranges from 1° to 6°, which was adjusted by utilizing the goniometer. When the incident angles match the mode coupling condition, the incident light will be coupled into the guided LN layer, leading to ATR on the reflected light spectrum. The peaks and troughs of multifarious polarized beams vary significantly from 5 different polarized beams at the same incident angle. Therefore, distinct polarized beams can be separated with each other by the PBA based on the DMCW.

According to experimental results, the pure TE or TM polarized beam can be distinguished, while variable proportions of TE and TM polarized beam is much more complicated. In this plan, the circular polarized light and elliptical light can be distinguished via monitoring the ATR of reflected spectrum at same scan range. As shown in Fig. 3(c), the ATR of circular polarized light reflected spectrum displays two same ATR dips between 5° to 5.5° At the same time, the light reflected spectrum presents two different dips at the same scan range from the two elliptical lights in Fig. 3(d) and Fig. 3(e). In this method, a variety of ratios of TE and TM polarization of incident lights are detected via the DCMW PBA as shown in Fig. 4(a). Eight reflected light curves for incident light with kinds of ratios of TM/TE=tan (10°, 20°, 30°, 40°, 50°, 60°, 70°, 80°) in experiments are plotted. Among the range of 4.9° to 5.2°, different polarization incident lights form distinct dips at coupling angles. Furthermore, as the ratio of TM/TE increases, the position of the ATR dip shifts and the coupling angle increases. As shown in picture, a monotony increasing trend means that incident lights with unique polarization components correspond to particular points on the graph. Moreover, eight dips in the picture are used to fit a curve, $y = -49.42 + 10.94x,\ (x \in [4.52, 5.43])$, which indicates the polarization intensity ratio of incident light. In theory, any point on this curve presents a ratio of TE/TM. In other words, arbitrary polarization intensity ratio can be detected. As shown above, TE and TM polarization show different modes in DMCW resulting in different ATR spectra. Moreover, various intensity ratios with TE and TM polarization will generate different ATR spectra. A table with coordinate values of troughs can be established. Hence, we can acquire the polarization ratio by parsing the look-up table. In real application, first of all, a well-made DMCW device will be calibrated with a series of known polarization beams which are varied in a continuous way. The matrices of polarization ratios and ATR data are acquired. By choosing a range of well-coupled angles (For example, 4.9° to 5.2° in Fig. 4a), a matrix in which polarization ratios correspond one-to-one with ATR dips is obtained. Then, we complete the calibration of this device. The polarization intensity ratio of incident light can be distinguished by the scanning of DMCW.

Actually, the sensitivity and accuracy of this device is not limited by DMCW, but restricted by photoelectric detector (PD). As shown in Fig. 4(b), the difference between TE and TM incident light is usually

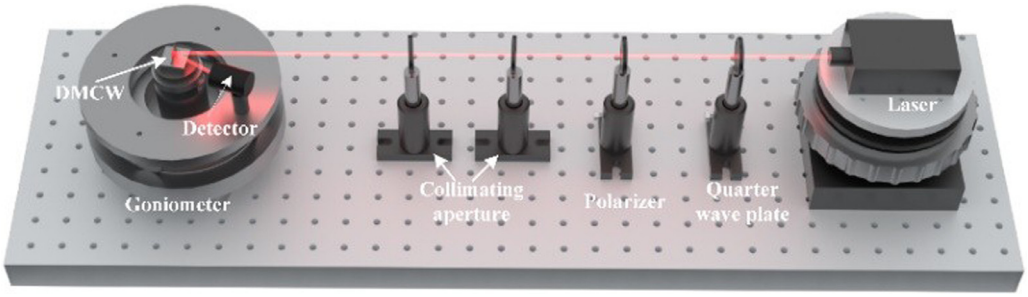

Fig. 2. Configuration of the experimental setup (DMCW, Goniometer, Detector, Collimating aperture, Polarizer, Quarter wave plate, 632.8 nm Laser).

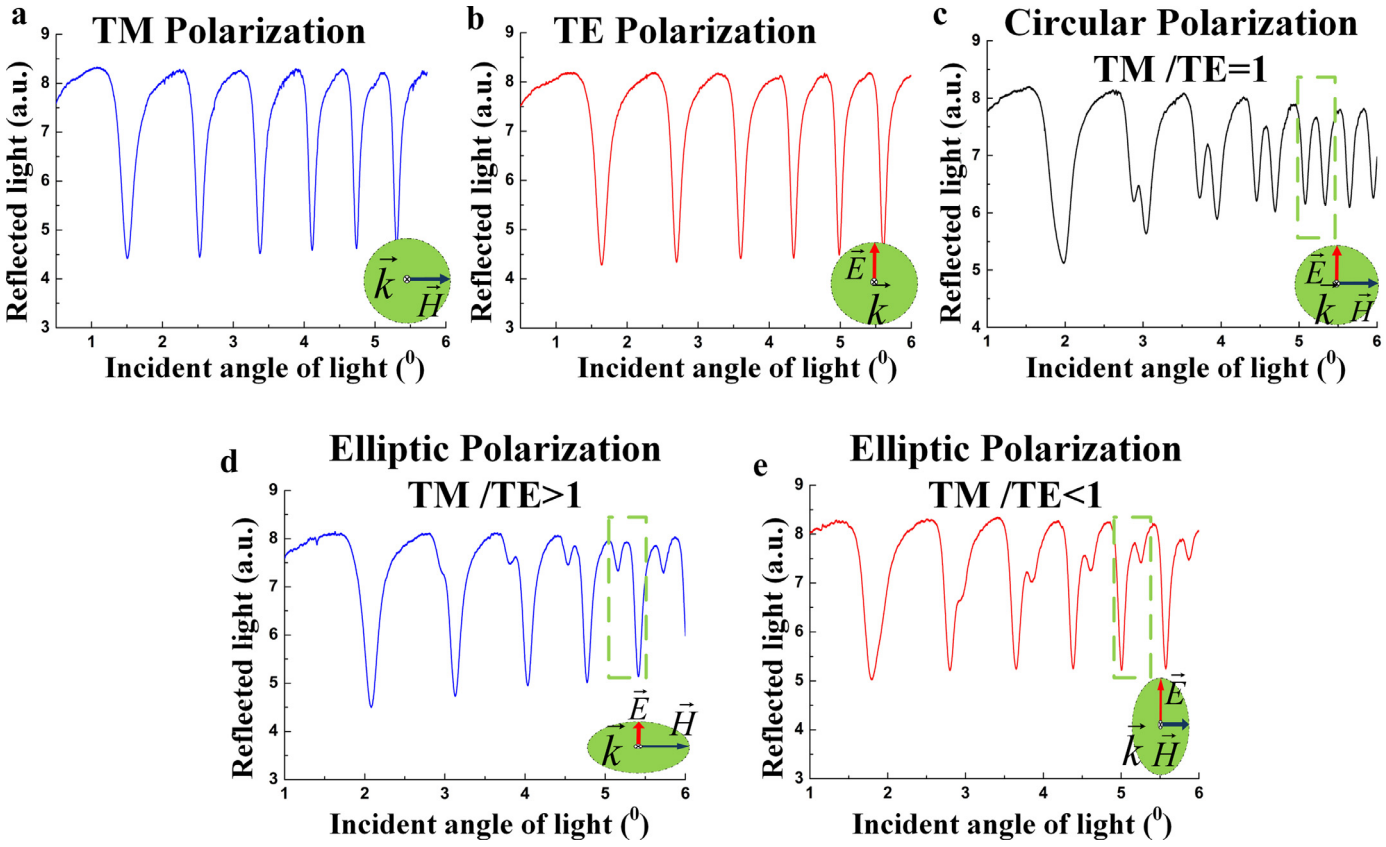

Fig. 3. Experimental verification of the proposed PAB method with distinct polarized beams at the wavelength of 632.8 nm. (a), (b) The experimental reflected light spectrum with pure TM and TE incident light, respectively. (c) The experimental reflected light spectrum with equal amounts of TM and TE. (d), (e) The experimental reflected light spectrum with different amounts of TM and TE.

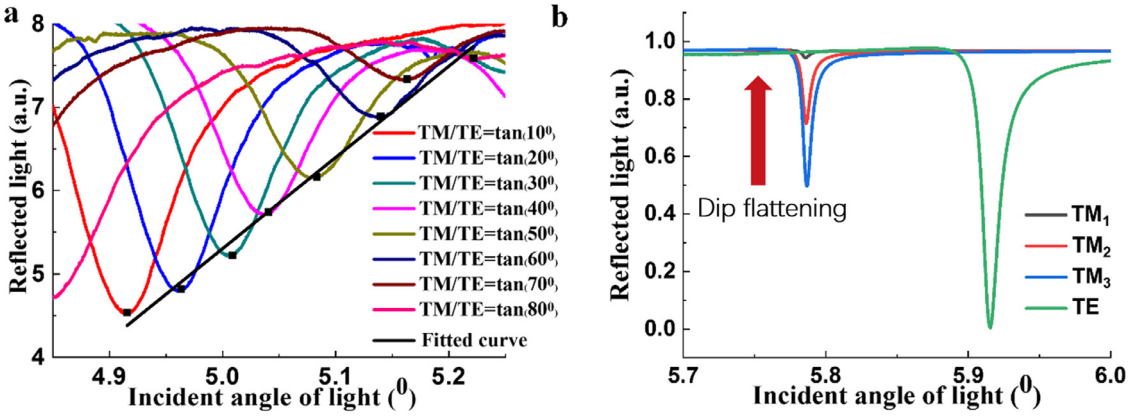

Fig. 4. (a) The experimental responses of the PBA based on DMCW with kinds of ratios of TM/TE=tan (10°,20°, 30°, 40°, 50°, 60°, 70°, 80°) at the wavelength of 638.2 nm. (b) Simulation about the different coupling angles with TE and TM. The red arrow shows increase of reflected intensity of TM.

greater than 0.1° well over the limit of 0.01° in DMCW. However, as the intensity of reflected light increase (for example TM), PD may fail to distinguish the input signal due to a flattening ATR dip. Hence, this device will always work whenever the reflected light can be monitored and recognized by the PD. Moreover, the isolation of our device is easy to reach 40dB According to the calculations in 632.8 nm at 5.7934° by ATR software, I_{TM}=5.6×10^{-5}, I_{TE}=0.987, and we get the isolation of I_{ISO}=42.46dB (I_{ISO}= −10lg (ITM/ITE), I_{TM}, I_{TE} are reflected light intensity of TM and TE, respectively.) And the measured isolation is determined by coupling efficiency of DMCW and the sensitivity of the photoelectric detector. In experiment, a DMCW with a 93.7% coupling efficiency and a photoelectric detector with a 10^5 dynamic range are used. The measured intensity of TM polarization is I_{TM}=0.012, and the intensity of TE polarization is I_{TE}=9.6. We acquire the isolation $I_{ISO} = -10\lg(I_{TM}/I_{TE}) = -10\lg(0.012/9.6) = 29.03\ dB$

Significantly, this method based on DMCW can be used in ultraviolet, visible, and infrared region, which is an excellent advantage for utilizing in many aspects. In the above experiments, a system designed for 632.8 nm, which contains a 35 nm silver film, a 0.5 mm LN layer, and a 300 nm silver film is proposed. Our device is effective as long as the two cladding layers exhibit metallic properties. By changing material and thick of cladding layers, the supported wavelength will extend more. In infrared and ultraviolet region, it will have reliable performance.

4. Discussion

In real applications, the surface of DMCW is not smooth as simulation. We calculate the ATR spectrum with surface roughness data from atomic force microscopy (AFM) images of DMCW. In perfect condition simulation, the full width at half maximum (FWHM) is 0.0149° With consideration of surface structure roughness, the FWHM become 0.0272°, which is broadened by 82%. Therefore, there is often a certain degree loss of resolution if the Ag films are fabricated roughly.

Another important thing in application is the irregularity of incident wave. For non-semi-plane wave incidence, we consider a situation with Gaussian incident beam which possesses variety of intensity and incident angles. In experiment, a collimating aperture with diameter of 1 mm which is one meter from DMCW is used to collimate the incident light. Hence, we choose a Gaussian beam with a 0.5 *mrad* divergence and 1 mm^2 spot area as incident wave. The ATR FWHM of Gaussian beam incidence grows from 0.0149° to 0.0335°,which is broadened by 125%. Therefore, incidence at beam waist is needed in real application in order to reduce wave irregularity error.

5. Conclusion

In summary, a new approach to generate a PBA using a DMCW is proposed and experimentally demonstrated. The PBA for 632.8 nm incident light with different orthogonal polarization intensity ratio is successfully realized. With effective separation of TE and TM incident light, an over 40 dB isolation can be obtained. Moreover, this method can be extended to infrared and ultraviolet region by changing the material of cladding layers. Our system is simple with free-space coupling and compact by using waveguide technology, presenting that it is very significant to the applications of optical information processing system and the integrated system.

Declaration of Competing Interest

The authors declare no conflicts of interest.

CRediT authorship contribution statement

Hongrui Shan: Formal analysis, Software, Writing – original draft. **Qiheng Wei:** Formal analysis. **Hailang Dai:** Methodology, Writing – original draft, Supervision. **Xianfeng Chen:** Conceptualization, Writing – review & editing.

Funding

National Key R&D Program of China (Grant Nos. 2017YFA0303701 and 2018YFA0306301); National Natural Science Foundation of China (NSFC) (11734011, 11764020, and 11974245); the Foundation for the fellowship of China Postdoctoral Science Foundation (2020M681275 and 2021T140452); Foundation for Development of Science and Technology of Shanghai (17JC1400400); and the Shanghai Municipal Science and Technology Major Project (Grant No. 2019SHZDZX01).

References

[1] Dai D, Liang D, Liu L. Introduction for the Integrated Photonics: challenges and Perspectives feature. Photonics Res. 2015;3.
[2] Wu F, Li G, Huang J, Yu D. Calcite/barium fluoride ultraviolet polarizing prism. Appl. Opt. 1995.
[3] Pang Y, Cao A, Wang J, Pang H, Yan W, Wu X, Shi L, Deng Q. Design and experimental verification of a monolithic complete-light modulator based on birefringent materials. Photonics Res. 2019:7.
[4] Wu W, Han P, Shi M, Su F, Wu F. Design and performance analysis of a single-unit polarizing beam-splitting prism based on negative refraction in a uniaxial crystal. Appl. Opt. 2019;58:7063–6.
[5] Yang S, Chen W, Nelson RL, Zhan Q. Miniature circular polarization analyzer with spiral plasmonic lens. Opt. Lett. 2009;34:3047–9.
[6] Azzam RMA, Adams RM. Transmission of p- and s-polarized light through a prism and the condition of minimum deviation. J. Opt. Soc. Am. A Opt. Image Sci. Vis. 2010;27:2085–90.
[7] Moreno I, Davis JA, Ruiz I, Cottrell DM. Decomposition of radially and azimuthally polarized beams using a circular-polarization and vortex-sensing diffraction grating. Opt. Express 2010;18:7173–83.
[8] Zhu C, Jiao Q, Tan X, Wang W, Bayanheshig. Design of a subwavelength all-metal grating for generating azimuthally polarized beams based on modified particle swarm optimization. Appl. Opt. 2019;58:4052–8.
[9] Bomzon ZE, Biener G, Kleiner V, Hasman E. Real-time analysis of partially polarized light with a space-variant subwavelength dielectric grating. Opt. Lett. 2002;27:188–90.
[10] Krishnan S, Hampton S, Rix J, Taylor B, Azzam RMA. Spectral polarization measurements by use of the grating division-of-amplitude photopolarimeter. Appl. Opt. 2003;42:1216–27.
[11] Li Z, Yao XS, Chen X, Chen H, Meng Z, Liu T. Complete Characterization of Polarization-Maintaining Fibers Using Distributed Polarization Analysis. J. Lightwave Technol. 2015;33:372–80.
[12] Mikhailov V, Rabin BA, Westbrook PS. In-Line High-Speed All-Fiber Polarimeter With True Real-Time Acquisition for Sensor Systems Based on Fast Polarization Rotation. J. Lightwave Technol. 2015;33:2679–84.
[13] Zhang Y, Zhang F, Pan S. Optical single sideband polarization modulation for radio-over-fiber system and microwave photonic signal processing. Photonics Res. 2014:2.
[14] Tang X, Liao J, Li H, Liu Y. Novel Approach for Controllable Polarization Beam Splitter: design and Simulation. IEEE J. Quantum Electron. 2013;49:43–50.
[15] Gan F, Sun C, Li H, Gong Q, Chen J. On-chip polarization splitter based on a multimode plasmonic waveguide. Photonics Res. 2017:6.
[16] Fukuda H, Wada K. Parallel-core-type polarization rotator for silicon wire waveguide platform. Photonics Res. 2014:2.
[17] Dai H, Yuan L, Yin C, Cao Z, Chen X. Direct Visualizing the Spin Hall Effect of Light via Ultrahigh-Order Modes. Phys. Rev. Lett. 2020;124.
[18] Hosain SI, Meunier JP, Bourillot E, Defornel F, Goudonnet JP. Review of the basic methods for characterizing integrated-optic waveguides. Fiber Integr. Opt. 1995;14:89–107.
[19] Li H, Cao Z, Lu H, Shen Q. Free-space coupling of a light beam into a symmetrical metal-cladding optical waveguide. Appl. Phys. Lett. 2003;83:2757–9.
[20] Dai H, Yin C, Ye X, Jiang B, Ran M, Cao Z, Chen X. A possible pathogenetic factor of sickle-cell disease based on fluorescent analysis via an optofluidic resonator. Sci. Rep. 2017;7:3174.
[21] Lu H, Cao Z, Li H, Shen Q. Study of ultrahigh-order modes in a symmetrical metal–cladding optical waveguide. Appl. Phys. Lett. 2004;85:4579–81.
[22] Zheng Y, Yuan W, Chen X, Cao Z. Wideband slow-light modes for time delay of ultrashort pulses in symmetrical metal-cladding optical waveguide. Opt. Express 2012;20:9409–14.
[23] Chen F, Cao Z, Shen Q, Deng X, Wang S. Picometer displacement sensing using the ultrahigh-order modes in a submillimeter scale optical waveguide. Opt. Express 2005;13:10061–5.
[24] Mukundan H, Anderson AS, Grace WK, Grace KM, Hartman N, Martinez JS, Swanson BI. Waveguide-based biosensors for pathogen detection. Sensors (Basel) 2009;9:5783–809.
[25] Zourob M, Mohr S, Brown BJT, Fielden PR, Mcdonnell M, Goddard NJ. The development of a metal clad leaky waveguide sensor for the detection of particles. Sensors Actuators B Chem. 2003;90:296–307.
[26] Wu W, Yu Y, Liu W, Zhang X. Fully integrated CMOS-compatible polarization analyzer. Nanophotonics 2019;8:467–74.
[27] Liu S, Qi S, Zhang Y, Li P, Wu D, Han L, Zhao J. Highly efficient generation of arbitrary vector beams with tunable polarization, phase, and amplitude. Photonics Res. 2018:6.

[28] Zourob M, Mohr S, Treves Brown BJ, Fielden PR, Mcdonnell MB, Goddard NJ. An integrated metal clad leaky waveguide sensor for detection of bacteria. Anal. Chem. 2005;77:232.
[29] Li X, Ma R, Xia Y. Magnetic Field Sensor Exploiting Light Polarization Modulation of Microfiber With Magnetic Fluid. J. Lightwave Technol. 2018;36:1620–5.
[30] Kullab HM, Taya SA, El-Agez TM. Metal-clad waveguide sensor using a left-handed material as a core layer. J. Opt. Soc. Am. B Opt. Phys. 2012;29:959–64.
[31] Taya SA, Kullab HM. Optimization of transverse electric peak-type metal-clad waveguide sensor using double-negative materials. Appl. Phys. A 2014;116:1841–6.
[32] Kazuhiro Hotta AY, Teramae N. Properties of A Metal Clad Waveguide Sensor Based on A Nanoporous-Metal-Oxide/Metal Multilayer Film. Anal. Chem. 2010;82:6066.
[33] Kullab HM, Taya SA. Transverse magnetic peak type metal-clad optical waveguide sensor. Optik - Int. J. Light Electron Opt. 2014;125:97–100.
[34] Chou Chau YF, Chou Chao CT, Huang HJ, Kumara N, Lim CM, Chiang HP. Ultra--High Refractive Index Sensing Structure Based on a Metal-Insulator-Metal Waveguide-Coupled T-Shape Cavity with Metal Nanorod Defects. Nanomaterials (Basel) 2019;9.